IEEE Photonics Journal
An IEEE Photonics Society Publication

Photonic Generation of Few-Cycle Millimeter-Wave Pulse Using a Waveguide-Based Photonic-Transmitter-Mixer

Volume 4, Number 4, August 2012

Jin-Wei Shi
J. W. Lin
C.-B. Huang
F.-M. Kuo
Nan-Wei Chen
Ci-Ling Pan
John E. Bowers

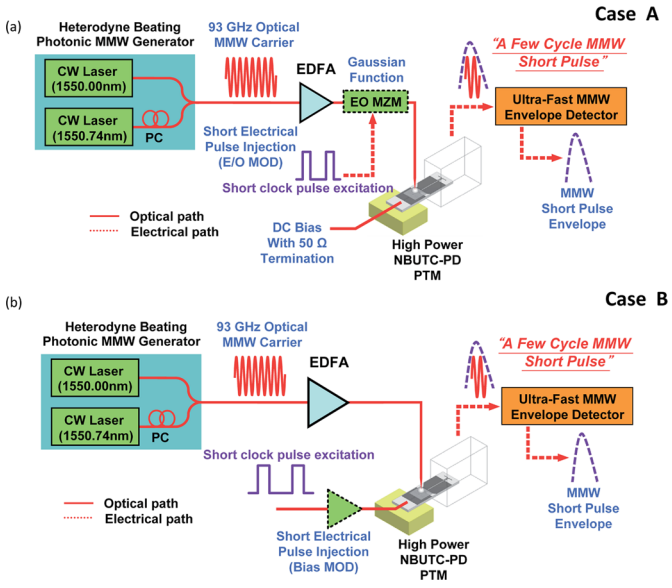

DOI: 10.1109/JPHOT.2012.2204733
1943-0655/$31.00 ©2012 IEEE

Photonic Generation of Few-Cycle Millimeter-Wave Pulse Using a Waveguide-Based Photonic-Transmitter-Mixer

Jin-Wei Shi,[1] J. W. Lin,[2] C.-B. Huang,[3] F.-M. Kuo,[1] Nan-Wei Chen,[4] Ci-Ling Pan,[2,3] and John E. Bowers[5]

[1]Department of Electrical Engineering, National Central University, Taoyuan 320, Taiwan
[2]Department of Physics, National Tsing Hua University, Hsinchu 30013, Taiwan
[3]Institute of Photonics Technologies, National Tsing-Hua University, Hsinchu 30013, Taiwan
[4]Department of Communications Engineering, Yuan Ze University, Taoyuan 320, Taiwan
[5]Electrical and Computer Engineering Department, University of California, Santa Barbara, CA 93106 USA

DOI: 10.1109/JPHOT.2012.2204733
1943-0655/$31.00 ©2012 IEEE

Manuscript received May 2, 2012; revised June 1, 2012; accepted June 6, 2012. Date of publication June 13, 2012; date of current version June 26, 2012. This work was supported by the National Science Council of Taiwan under Grant NSC-100-2918-I-008-004 and Grant 98-2221-E-007-026-M3 and by the Defense Advanced Research Projects Agency MTO PICO project. Corresponding author: J.-W. Shi (e-mail: jwshi@ee.ncu.edu.tw).

Abstract: We demonstrate a novel technique for photonic generation of few-cycle millimeter-wave (MMW) pulse using a WR-10 waveguide and near-ballistic unitraveling carrier photodiode (NBUTC-PD)-based photonic-transmitter-mixer (PTM). A 2.5-cycle MMW pulse is generated by simultaneously exciting the PTM optical port with ~100-GHz optical MMW sinusoidal signal and the intermediate-frequency (IF) port with a 25-ps electrical short pulse, respectively. Compared to results using femtosecond optical short pulses to directly excite the PTM (without E-O signal mixing), our approach is capable of providing much less signal distortion, eliminating the ringing oscillation in the tail of response, a much shorter pulse duration, and a higher peak power.

Index Terms: Microwave photonics, photodetectors.

1. Introduction

The generation of ultrashort electrical pulses in either free space or transmission lines through the photonic approach has been widely investigated over the past 40 years [1]–[4]. Optical rectification is a commonly employed method in obtaining sub-picosecond electrical pulses when nonlinear optical devices are excited by femtosecond optical pulses [5]. Alternatively, photoconductive antennas are also widely used [5]. Compared with the pure electronic approach for generation of sub-Terahertz (THz) electrical transients [6], [7], the major advantage of the photonic scheme is that the optical millimeter-wave (MMW) signal can be distributed to remote distances through low-loss optical fibers for making connections and/or synchronization of the entire system [4]. Some related applications, such as THz time-domain spectroscopy (TDS) [2], [8], [9], THz imaging [10], [11], and very-fast analog-to-digital (A-D)/digital-to-analog (D-A) converter [12], [13], have also been demonstrated. However, the generated sub-THz power in these techniques is usually too small and hinders further improvement in the system performance. The most straightforward solution to this low-power issue is to photonically generate the short electrical transients in a sub-MMW waveguide,

where the ensuing signal amplification and processing are feasible through the use of commercially available waveguide-based active/passive MMW components.

Despite such advantages, a waveguide is effectively a passive bandpass filter. Such bandpass nature causes detrimental loss, waveform distortion, ringing oscillation and pulse broadening when a short photogenerated electrical pulse (covering frequency range from nearly DC to sub-THz) propagates down a waveguide. In addition, photodiodes and other active MMW components in generating the short pulses can be easily saturated by the high peak-power. One possible way to overcome the aforementioned problems is to utilize the MMW chirped pulse generation technique [14]–[16]. However, a complex topology in the receiver architecture is required to recompress the long (tens of microseconds) chirped pulse back into near transform-limited duration (sub-ps) in order to provide a high temporal resolution. The ability to photonically generate high power, few-cycle MWM short pulse through a MMW waveguide is an attractive way in realizing a real-time, high-frame-rate, and high-temporal-resolution MMW radar system without the need for complex signal processing in the receiver. Compared with the MMW chirped pulse radar, although the maximum sensing distance of very-short pulse radar is more seriously limited by the peak output power of next stage MMW power amplifier (or oscillator) [17], this would not be a key issue for its application of bio-medical imaging system. Where, the radar imaging is constructed by the strong interaction between injected sub-MMW and in vivo hydration process [10]. The temporal resolution and frame rate (instead of sensing distance) both play important roles in such kind of radar imaging system. Furthermore, in order to further improve the maximum sensing distance of the proposed short-pulse radar system, a traveling-wave tube or magnetron-based oscillator with a very-high peak saturation power (under pulse-mode operation) integrated with our PTM is necessary [17]. For such case, our reported photonic MMW pulse generation technique also possesses the unique advantage of excellent isolation between input local oscillator (LO: sinusoidal MMW signal in optical domain) and output radio-frequency (RF: MMW pulse signal in electrical domain) signals while maintaining a short pulse width.

In this paper, we experimentally demonstrate a novel scheme for photonic generation of few-cycle MMW short pulses at the W-band using a WR-10 waveguide-based photonic-transmitter-mixer (PTM) [18], [19]. In our proposed method, a 2.5-cycle 93 GHz MMW pulse is generated by mixing an optical 93 GHz optical sinusoidal waveform and a 25 ps electrical pulse through a WR-10 waveguide. In our current demonstration, the 93 GHz sinusoidal waveform is derived through heterodyne beating of two CW lasers; and the 25 ps electrical pulse is obtained through laser intensity modulation using a $LiNbO_3$ modulator of our PTM. Compared with the results using fs optical short pulse to directly excite the PTM (without electrical-to-optical (E-O) signal mixing), which is also discussed in this paper, our proposed approach is capable of providing much less signal distortion, a much shorter pulse duration, and higher peak power. Furthermore, we demonstrate that signal mixing through our PTM module is beneficial in eliminating the use of an external modulator integrated with a high-power RF amplifier, canceling the ringing oscillation in the tail of MMW pulse. This approach offers the narrowest pulse width among all the discussed techniques in this paper.

2. TDS Measurement Setups and Results

A near-ballistic unitraveling carrier photodiode [20]–[22]-based photonic transmitter-mixer (PTM) at W-band, which has a wide intermediate frequency (IF) modulation bandwidth ($\sim$25 GHz) and an ultrawide optical-to-electrical (O-E) bandwidth (68–128 GHz), was adopted to convert the optical envelope to a MMW signal [19]. Compared with UTC-PD-based PTM [23], the NBUTC-PD-based PTM can provide a larger extinction (on/off) ratio ($>$ 20 dB), a smaller driving voltage [$\sim$1 V peak-to-peak (V_{pp})], and a much faster modulation speed due to the elimination of forward bias operation during switching and the dramatic variation in overshoot drift-velocity of electrons with electric field [24]. Figs. 1 and 2 show the schematics of our two different experimental setups for pulse generation. In Fig. 1, there is the THz time-domain spectroscopic (TDS) system [2], [8], [9], where, we excite our PTM with a femtosecond optical pulse to directly generate the short electrical pulse

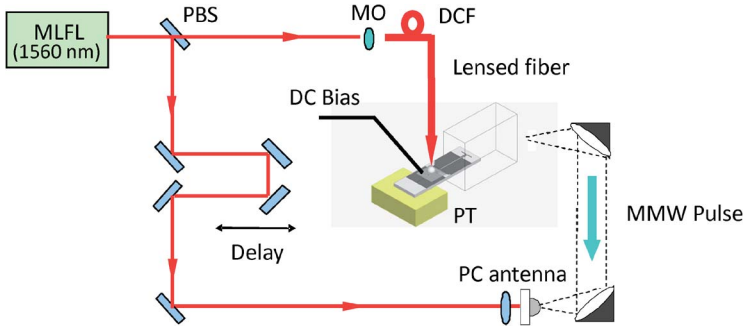

Fig. 1. Measurement setup for the TDS system. DCF: dispersion compensation fiber. PT: photonic-transmitter. MO: microscope objectives. PBS: polarization beam splitter. MLFL: mode-locked fiber laser. PC: photoconductive.

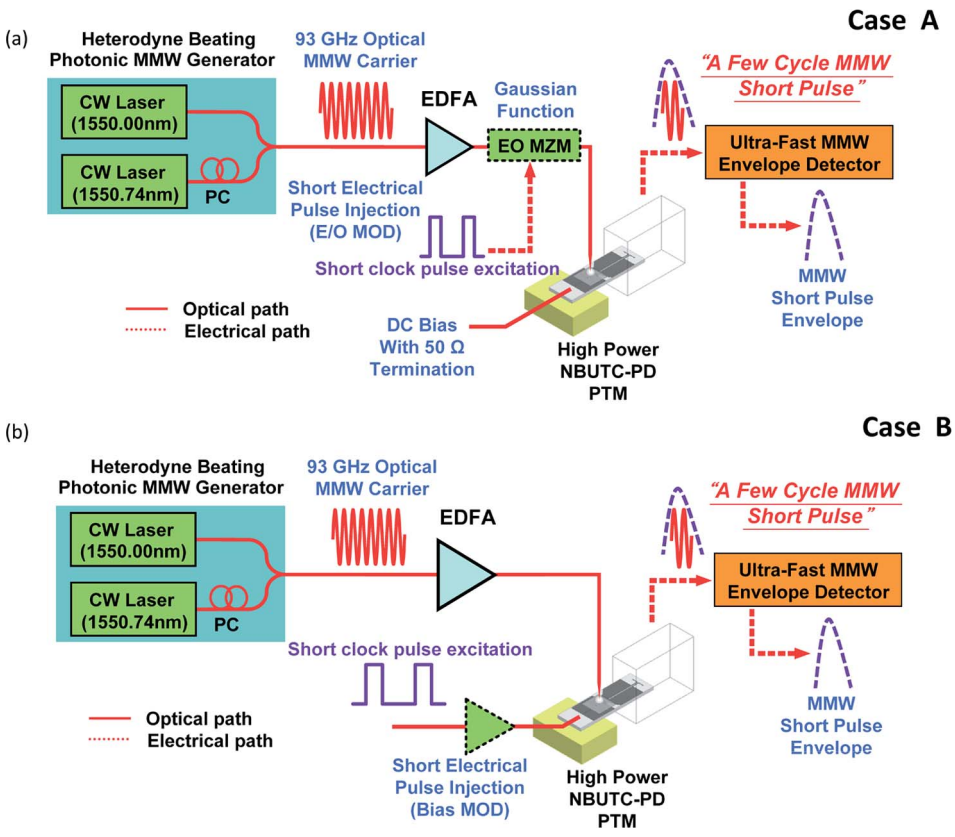

Fig. 2. Measurement setup for the demonstrated MMW short-pulse generation system. E-O MZM: electrooptic Mach–Zehnder modulator. MOD: modulation.

through the WR-10 waveguide [25]. The central wavelength, repetition rate, and optical pulse width of the fiber mode-locked laser are 1560 nm, 100 MHz, and 150 fs, respectively. The generated electrical transient is radiated through a WR-10 horn antenna and detected by an $In_{0.53}Ga_{0.47}As$-based photoconductive switch driven by the femtosecond optical pulse. For such application, the IF port of our PTM is left as open and the whole device functions as a simple ultrahigh speed photodiode, which converts the injected optical pulse into an electrical signal and has no frequency up-conversion or mixing processes inside. The generated electrical pulse usually has a Gaussian-like waveform and a broad frequency ranging from DC to hundreds of GHz [26], [27]. Some of the

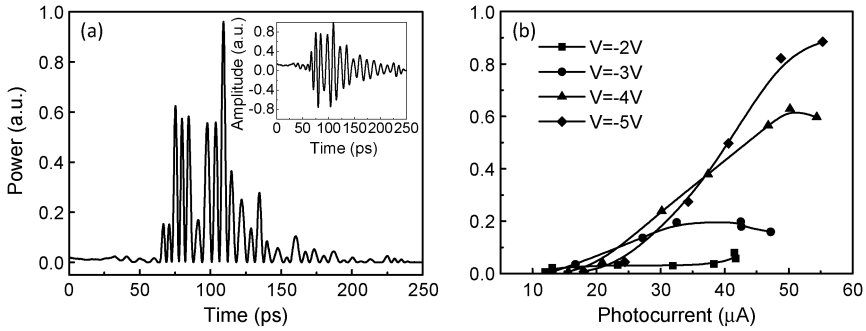

Fig. 3. Measured TDS power waveform (a) and the measured peak power of TDS waveform versus the averaged photocurrent (b). The inset in (a) shows the original measured trace without square.

frequency components of such radiated pulse, however, would be truncated after passing the bandpass WR-10 waveguide.

Fig. 3(a) shows the measured sub-THz power waveform from our device, which is obtained by squaring the measured amplitude waveform. The inset in Fig. 3(a) shows these original measured waveforms. As can be seen, the measurement result is in contrast to the measured impulse response of a typical wideband photodiode. The measured pulse width of envelope (with MMW carrier inside) is comparatively broad and has several cycles of W-band carrier-wave inside. This is because that the generated electrical pulse from our NBUTC-PD suffers from serious broadening and distortion after passing the bandpass WR-10 waveguide and the passive MMW circuits in the PTM module. Fig. 3(b) shows the normalized peak power of measured sub-THz waveform versus the output averaged photocurrent. We can clearly see that the value of maximum peak amplitude (saturation current) gradually increases with the reverse bias voltage. It indicates that the peak space-charge electric field, which is induced by the injected optical short pulse, seriously limits the peak output voltage from our NBUTC-PD [28]. Under the highest bias voltage (-5 V), the maximum generated charge per pulse is up to 550 fC (femto Coulomb). Compared with the other approaches using optical pulse excitation (Fig. 2), the MMW pulse generated by directly using a femtosecond optical short pulse excitation has a broader pulse width ($\sim$50 versus $\sim$37.4 ps) and contains fewer charges per pulse (550 fC versus 2800 fC).

3. Bias Modulation Measurement Setups and Results

In order to overcome the limitations in pulse width and the peak amplitude by pulsed excitation, we have proposed another solution, which is shown in Fig. 2(a). In this setup, the continuous optical MMW signal at 93 GHz is simply generated by the heterodyne beating technique. Although the generated MMW carrier wave by use of such technique may have a higher phase noise than that of high-performance electronic MMW frequency synthesizer, numerous techniques about phase-locking two free running lasers have been reported to further suppress the phase noise of photogenerated MMW signal [29]–[31]. In order to get the short-pulse waveform, two different schemes (A and B) have been adopted. In scheme A, we use a $LiNbO_3$-based external E-O modulator (MOD) to mix the continuous 93 GHz sinusoidal signal with the short electrical pulse (square wave) with a 25 ps pulse width, which is generated by the pulse pattern generator. We can thus expect that the output from the E-O MOD is an optical pulse (envelope) with a pulse width at around 25 ps and a few cycles of 93 GHz carrier inside. An additional high-power RF amplifier is necessary in this scheme to amplify the input 25 ps electrical pulse to the output level with peak amplitude at $\sim$5 V for driving the E-O MOD. Another approach (scheme B) is to use the ultrafast modulation characteristic [18], [19] of our PTM to generate the MMW pulse. As shown in Fig. 2, the 25 ps electrical pulse from our PPG directly input to the IF port of our PTM. Due to the driving-voltage of our PTM is as small as 1 V (for $>$ 20 dB MMW power variation), the additional high-power

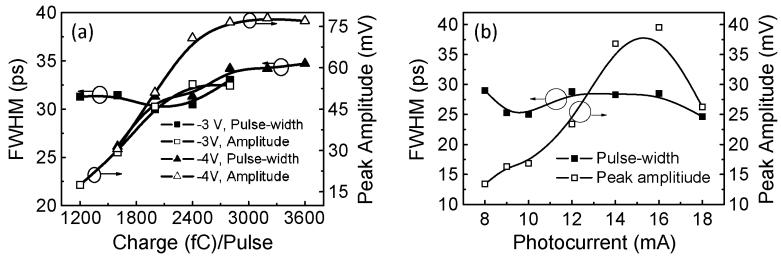

Fig. 4. FWHM (after de-embedding the receiver time resolution) and peak amplitude of the measured envelope of the MMW pulse versus output charge per pulse and output CW photocurrent (under different reverse bias voltages) for (a) optical pulses excitation (scheme A) and (b) bias modulation (scheme B).

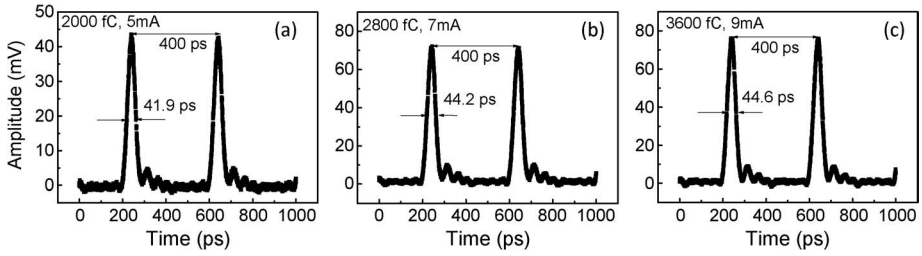

Fig. 5. Measured envelope waveform (without de-embedding the receiver time resolution) of MMW pulse under a fixed reverse bias voltage (~ -4 V) and different output charges per pulse for (a) 2000 fC (5mA averaged current), (b) 2800 fC (7 mA averaged current), and (c) 3600 fC (9 mA averaged current).

RF driving amplifier can thus be eliminated. The transfer curve of photogenerated MMW power versus reverse bias voltage of our PTM is given in our previous work [22].

In the receiver-end, we use a very-fast MMW power detector, which has around 37 GHz of video bandwidth [19], to directly detect the envelope of emitted MMW pulses through the WR-10 waveguide. In contrast to the periodic (cosine) transfer function of E-O MOD, the transfer curve (MMW power versus reverse bias voltage) of PTM is highly nonlinear with a small driving voltage V_{pp} (1 V) and a large extinction ratio ($>$ 20 dB) [22]. This characteristic of PTM would sharpen the generated MMW pulse and benefit the short-pulse generation, as will be discussed later. In addition, another main difference between scheme A and B is their different operation modes of the PTM. In scheme A, the PTM is excited by an optical pulse train from the EO-MOD and thus under pulse-mode operation. On the other hand in scheme B, during bias modulation, the output DC photocurrent from the PTM remains unchanged and its maximum saturation current is the same as the case of continuous wave (CW) operation [18], [19]. The generated MMW pulse (envelope) is due to the change in device speed performance (electron drift-velocity) under the switching of reverse bias voltage onto the device.

Fig. 4(a) and (b) show the full-width at half-maximum (FWHM) and peak amplitude of the measured envelope of MMW pulse versus output charges per pulse (or CW photocurrent) of scheme A and B, respectively. The injected electrical pulse train into IF port of PTM or EO-MOD has a pulse width fixed at 25 ps and the same 400 ps repetition time for both cases. By pre-biasing our PTM under around -1 V DC voltage with around 1 V peak-to-peak IF driving voltage, we can get the largest amplitude of generated MMW pulse. This result is consistent with the transfer curve of PTM [22], which exhibits significant variation in MMW power when the reverse bias switches from -1 to -2 V [22]. Here, we assume that the fast MMW detector in our receiver has a Gaussian-shape impulse response with a 28 ps FWHM, which corresponds to its 37 GHz video bandwidth [19]. The values of FWHM shown in Fig. 4 have been deconvoluted with such a time constant. Figs. 5 and 6 show the original measured waveforms (without deconvolution of the response of the

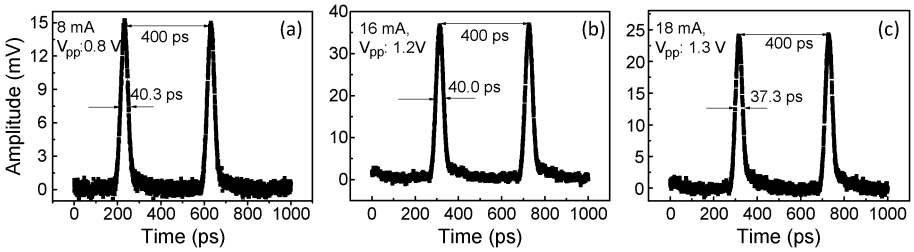

Fig. 6. Measured envelope waveform (without de-embedding the receiver time resolution) of the MMW pulse under a fixed reverse bias voltage (-1 V) and different output photocurrents of (a) 8 mA, (b) 16 mA, and (c) 18 mA. The IF driving voltage (V_{pp}) for cases (a) to (c) has been optimized for narrowest FWHM and highest peak amplitude.

fast power detector) at different output photocurrents (or charge per pulse) for schemes A and B with narrowest pulse widths, respectively.

As can be seen, the dynamic behavior of the measured impulse responses under such two operation modes (A and B) is very different. In scheme A, the maximum peak amplitude and saturation current (charge per pulse) of the generated pulse are significantly enhanced with increasing reverse bias voltage (-3 to -4 V). Furthermore, when the output charge per pulse is below 2000 fC (8 mA photocurrent), the measured FWHM decreases significantly with increasing reverse bias voltage (-3 to -4 V). Overall, in order to minimize broadening of the impulse response and achieve the highest possible peak output amplitude, the increase in reverse bias voltage (-3 to -4 V) is necessary. These measurement results are similar with the PD under pulse-mode operation as discussed in Figs. 1 and 3. The maximum generated charge per pulse is as high as 2800 fC with a $\sim$33 ps deconvoluted pulse width and a 75 mV peak output amplitude. Such performance is superior to the TDS measurement result, which shows a 550 fC charge per pulse with a 50 ps pulse width, as shown in Fig. 1. This can be attributed to the fact that the generated optical MMW envelope by use of scheme A has a frequency component centered at 93 GHz with a $\sim$30 GHz bandwidth, which is well within the working bandwidth of WR-10 waveguide (75–110 GHz). Less distortion and broadening of generated pulse after passing through the waveguide can thus be achieved compared with that of the TDS technique. In the TDS setup, the PTM was excited by an optical pulse with a frequency component ranging from DC to hundreds of GHz. Furthermore, the improvement in output power (charge per pulse) is mainly due to the fact that the peak optical power of the pulse generated by the EO-MOD is much lower than that of the mode-locked laser in the TDS system. This would minimize the saturation of PTM under a high peak optical power excitation [28]. On the other hand, for case B, the measured FWHM of pulse shows no significant broadening with the increase of CW output photocurrent. This can be attributed to the bandwidth enhancement effect of NBUTC-PD under high current CW operation [32], [33]. An $\sim$28 ps pulse width with the 40 mV peak amplitude can be achieved by use of scheme B. By use of the value of averaged photocurrent and the measured waveform of MMW impulse response, as shown in Fig. 5, we can estimate the values of peak output photocurrent, actual peak output power from our PTM, and the dynamic sensitivity of our fast MMW envelope detector. According to our calculation and measurement results, the dynamic sensitivity of our detector is around 1 V/W and the highest peak output power of scheme A and B is around 78 and 40 mW, respectively. Although the peak power of the measured response by using the bias modulation technique (scheme B) is smaller than that of scheme A (40 versus 78 mW), it provides a narrower impulse response (28.5 versus 37.4 ps). Furthermore, as shown in Figs. 5 and 6, the ringing oscillation in the tail of measured impulse responses under optical pulse excitation can be completely eliminated by use of bias modulation. This is an important issue for radar applications due to the fact that such ringing oscillation might mix with the reflected waves and have serious influence on the echo signals from objects under measurement. The superior performance of the bias modulation technique to optical pulse excitation may be attributed to the fact that the NBUTC-PD PTM provides a sharp transfer function [21] and it can further sharpen the generated MMW pulse. Compared with the reported MMW chirped pulse generation technique with state-of-the-art

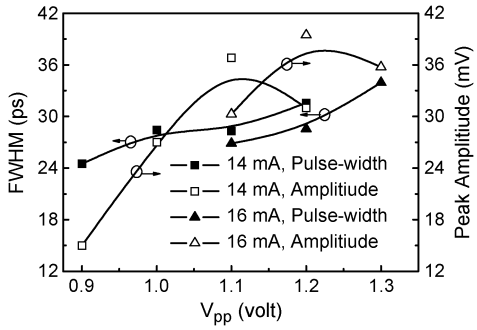

Fig. 7. FWHM (after de-embedding the receiver time resolution) and peak amplitude of the measured envelope of the MMW pulse versus IF driving voltage (V_{pp}) under different output photocurrents (14 and 16 mA) for scheme B.

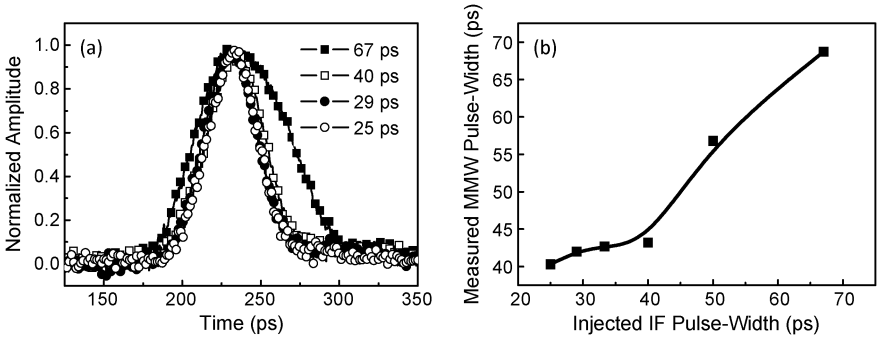

Fig. 8. (a) The measured envelope waveforms (without de-embedding the receiver time resolution) of the MMW pulses obtained using scheme B with different electrical pulse widths injected to the IF port. (b) The corresponding FWHMs of the measured MMW envelope versus injected pulse width.

compression ratio (89–103 GHz/50 μs/7 $\times$ 10^5) [16], our photonic MMW short pulse technique can offer a larger bandwidth ($\sim$26 GHz (38 ps) versus 14 GHz) at the same carrier wave frequency ($\sim$93 GHz), which indicates a higher temporal resolution.

In addition, the value of peak-to-peak IF driving voltage plays an important role in the output amplitude of the MMW pulse for case B under high output photocurrent ($>$ 10 mA). Fig. 7 shows the measured peak amplitude and pulse width versus IF driving voltage under different output photocurrents. As can be seen, an optimized IF driving voltage for the maximum peak output amplitude exists and this optimum driving voltage increases with the increase in output photocurrent. As can be seen, when the output photocurrent increases from 14 to 16 mA, the optimum V_{pp} increases from 1.1 to 1.2 V and the further increase in V_{pp} would lead a significant degradation in both output amplitude and pulse width. The existence of optimized IF driving-voltage is due to the fact we must switch our PTM in the most linear regime of the transfer curve to get the narrowest pulse width with high peak-output power. The increase in this value with photocurrent is mainly due to the fact that a larger IF voltage swing is necessary to compensate the shift in DC operation point and the change in transfer curve under a high output DC photocurrent operation.

Phase and amplitude coding of the MMW pulse plays an important role to further enhance the resolution of radar image [34]. By use of our proposed bias modulation technique (scheme B), the generated MMW pulse width can be easily controlled by the injected electrical pulse width to the IF port of our PTM. Fig. 8(a) shows the measured waveform of impulse responses by use of scheme B (bias modulation) with different electrical pulse width injected to the IF port. Fig. 8(b) shows the corresponding pulse width of measured MMW impulse response versus those of injected pulses to the IF port. As can be seen, when the injected IF pulse width is reduced from 70 to 40 ps, the

generated MMW pulse width decreases significantly. On the other hand, when the injected IF pulse width is narrower than 40 ps, the reduction in generated MMW pulse width becomes insignificant. This phenomenon is mainly due to that the generated MMW pulse width (impulse response) is eventually limited by the modulation bandwidth of our IF port (25 GHz) and the video bandwidth of our envelope detector ($\sim$37 GHz) [18]. The decrease in generated MMW pulse width thus becomes negligible by further reducing the injected IF pulse width ($<$ 40 ps).

4. Conclusion

In conclusion, we have demonstrated a novel photonic MMW short pulse generation technique using a MMW waveguide. Compared with exciting the photonic transmitter by a femtosecond optical short pulse to directly generate the short electrical transient, the generated MMW pulses by use of our approaches can have a higher peak output power, less distortion through waveguide, and a narrower pulse width. In our new approaches, the external high-speed E-O MOD or the IF bias modulation port of our PTM is used to mix the continuous optical MMW signal at W-band with the envelope of short electrical pulse train. As compared to using the high-speed (40 Gbit/sec) E-O MOD under pulse-mode operation, the bias modulation technique can provide the narrowest MMW pulse width among all the discussed techniques and kill the ringing oscillation in the tail of generated short MMW pulse due to the ultrafast bias modulation characteristic and the sharp transfer function of our PTM.

References

[1] D. H. Auston, "Picosecond optoelectronic switching and gating in silicon," *Appl. Phys. Lett.*, vol. 26, pp. 101–103, Feb. 1975.

[2] D. R. Grischkowsky, "Optoelectronic characterization of transmission lines and waveguides by terahertz time-domain spectroscopy," *IEEE J. Sel. Topics Quantum Electron.*, vol. 6, no. 6, pp. 1122–1135, Nov./Dec. 2000.

[3] M. Y. Frankel, S. Gupta, J. A. Valdmanis, and G. A. Mourou, "Terahertz attenuation and dispersion characteristics of coplanar transmission lines," *IEEE Trans. Microw. Theory Tech.*, vol. 39, no. 6, pp. 910–916, Jun. 1991.

[4] T. Nagatsuma, M. Shinagawa, N. Sahri, A. Sasaki, Y. Royter, and A. Hirata, "1.55-μm photonic systems for microwave and millimeter-wave measurement," *IEEE Trans. Microw. Theory Tech.*, vol. 49, no. 10, pp. 1831–1839, Oct. 2001.

[5] M. Tonouchi, "Cutting edge terahertz technologies," *Nat. Photon.*, vol. 1, pp. 97–105, Feb. 2007.

[6] M. J. W. Rodwell, S. T. Allen, R. Y. Yu, M. G. Case, U. Bhattacharya, M. Reddy, E. Carman, M. Kamegawa, Y. Konishi, J. Pusl, and R. Pullela, "Active and nonlinear wave propagation devices in ultrafast electronics and optoelectronics," *Proc. IEEE*, vol. 82, no. 7, pp. 1037–1059, Jul. 1994.

[7] U. Bhattacharya, S. T. Allen, and M. J. W. Rodwell, "DC-725 GHz sampling circuits and subpicosecond nonlinear transmission lines using elevated coplanar waveguide," *IEEE Microw. Guided Wave Lett.*, vol. 5, no. 2, pp. 50–52, Feb. 1995.

[8] T.-A. Liu, G.-R. Lin, Y.-C. Chang, and C.-L. Pan, "Wireless audio and burst communication link with directly modulated THz photoconductive antenna," *Opt. Exp.*, vol. 13, no. 25, pp. 10 416–10 423, Dec. 2005.

[9] Y.-T. Li, J.-W. Shi, C.-Y. Huang, N.-W. Chen, S.-H. Chen, J.-I. Chyi, Y.-C. Wang, C.-S. Yang, and C.-L. Pan, "Characterization and comparison of GaAs/AlGaAs uni-traveling carrier and separated-transport-recombination photodiode based high-power sub-THz photonic-transmitters," *IEEE J. Quantum Electron.*, vol. 46, no. 1, pp. 19–27, Jan. 2010.

[10] Z. D. Taylor, R. S. Singh, D. B. Bennett, P. Tewari, C. P. Kealey, N. Bajwa, M. O. Culjat, A. Stojadinovic, H. Lee, J.-P. Hubschman, E. R. Brown, and W. S. Grundfest, "THz medical imaging: *In vivo* hydration sensing," *IEEE Trans. Terahertz Sci. Technol.*, vol. 1, no. 1, pp. 201–219, Sep. 2011.

[11] A. Dobroiu, M. Yamashita, Y. N. Ohshima, Y. Morita, C. Otani, and K. Kawase, "Terahertz imaging system based on a backward-wave oscillator," *Appl. Opt.*, vol. 43, no. 30, pp. 5637–5646, Oct. 2004.

[12] R. Urata, L. Y. Nathawad, R. Takahashi, K. Ma, D. A. B. Miller, B. A. Wooley, and J. S. Harris, Jr., "Photonic A/D conversion using low-temperature-grown GaAs MSM switches integrated with Si-CMOS," *IEEE/OSA J. Lightw. Technol.*, vol. 21, no. 12, pp. 3104–3115, Dec. 2003.

[13] G. C. Valley, "Photonic analog-to-digital converters," *Opt. Exp.*, vol. 15, no. 5, pp. 1955–1982, Mar. 2007.

[14] C. M. Long, D. E. Leaird, and A. M. Weiner, "Photonically enabled agile rf waveform generation by optical comb shifting," *Opt. Lett.*, vol. 35, no. 23, pp. 3892–2894, Dec. 2010.

[15] M. Li and J. P. Yao, "Photonic generation of continuously tunable chirped microwave waveforms based on a temporal interferometer incorporating an optically-pumped linearly-chirped fiber Bragg grating," *IEEE Trans. Microw. Theory Tech.*, vol. 59, no. 12, pp. 3531–3537, Dec. 2011.

[16] J.-W. Shi, F.-M. Kuo, N.-W. Chen, S. Y. Set, C.-B. Huang, and J. E. Bowers, "Photonic generation and wireless transmission of linearly/nonlinearly continuously tunable chirped millimeter-wave waveforms with high time-bandwidth product at W-band," *IEEE Photon. J.*, vol. 4, no. 1, pp. 215–223, Feb. 2012.

[17] M. A. Richards, J. A. Scheer, and W. A. Holm, *Principles of Modern Radar: Basic Principles*. Raleigh, NC: SciTech, 2010.

[18] F.-M. Kuo, C.-B. Huang, J.-W. Shi, N.-W. Chen, H.-P. Chuang, J. E. Bowers, and C.-L. Pan, "Remotely up-converted 20 Gbit/s error-free wireless on-off-keying data transmission at W-band using an ultra-wideband photonic transmitter-mixer," *IEEE Photon. J.*, vol. 3, no. 2, pp. 209–219, Apr. 2011.
[19] F.-M. Kuo, J.-W. Shi, N.-W. Chen, J. Hesler, and J. E. Bowers, "25 Gbit/s error-free wireless on-off-keying data transmission at W-band using ultra-fast photonic transmitter-mixers and envelop detectors," in *Proc. OFC*, Los Angeles, CA, Mar. 2012, p. OTh1E.5.
[20] J.-W. Shi, F.-M. Kuo, C.-J. Wu, C. L. Chang, C. Y. Liu, C.-Y. Chen, and J.-I. Chyi, "Extremely high saturation current-bandwidth product performance of a near-ballistic uni-traveling-carrier photodiode with a flip-chip bonding structure," *IEEE J. Quantum Electron.*, vol. 46, no. 1, pp. 80–86, Jan. 2010.
[21] F.-M. Kuo, M.-Z. Chou, and J.-W. Shi, "Linear-cascade near-ballistic uni-traveling-carrier photodiodes with an extremely high saturation-current-bandwidth product," *IEEE/OSA J. Lightw. Technol.*, vol. 29, no. 4, pp. 432–438, Feb. 2011.
[22] J.-W. Shi, F.-M. Kuo, and J. E. Bowers, "Design and analysis of ultra-high speed near-ballistic uni-traveling-carrier photodiodes under a 50 Ω load for high-power performance," *IEEE Photon. Technol. Lett.*, vol. 24, no. 7, pp. 533–535, Apr. 2012.
[23] A. Hirata, T. Furuta, H. Ito, and T. Nagatsuma, "10-Gb/s millimeter-wave signal generation using photodiode bias modulation," *J. Lightw. Technol.*, vol. 24, no. 4, pp. 1725–1731, Apr. 2006.
[24] F.-M. Kuo, Y.-L. Ho, J.-W. Shi, N.-W. Chen, W.-J. Jiang, C.-T. Lin, J. Chen, C.-L. Pan, and S. Chi, "12.5-Gb/s wireless data transmission by using bias modulation of NBUTC-PD based W-band photonic transmitter-mixer," in *Proc. OFC 2010*, San Diego, CA, Mar. 2010, p. OThF7.
[25] F.-M. Kuo, Y.-T. Li, J.-W. Shi, S.-N. Wang, N.-W. Chen, and C.-L. Pan, "Photonic impulse-radio wireless link at W-band using a near-ballistic uni-traveling-carrier photodiode-based photonic transmitter-mixer," *IEEE Photon. Technol. Lett.*, vol. 22, no. 2, pp. 82–84, Jan. 2010.
[26] H. Ito, T. Furuta, S. Kodama, N. Watanabe, and T. Ishibashi, "Inp/InGaAs uni-travelling-carrier photodiode with 310 GHz bandwidth," *Electron. Lett.*, vol. 36, no. 21, pp. 1809–1810, Oct. 2000.
[27] J.-W. Shi, K. G. Gan, Y. J. Chiu, Y.-H. Chen, C.-K. Sun, Y. J. Yang, and J. E. Bowers, "Metal-semiconductor-metal travelling-wave-photodetectors," *IEEE Photon. Technol. Lett.*, vol. 13, no. 6, pp. 623–625, Jun. 2001.
[28] P.-L. Liu, K.-J. Williams, M. Y. Frankel, and R. D. Esman, "Saturation characteristics of fast photodetectors," *IEEE Trans. Microw. Theory Tech.*, vol. 47, no. 7, pp. 1297–1303, Jul. 1999.
[29] Z.-F. Fan and M. Dagenais, "Optical generation of a megahertz-linewidth microwave signal using semiconductor lasers and a discriminator-aided phase-locked loop," *IEEE Trans. Microw. Theory Tech.*, vol. 45, no. 8, pp. 1296–1300, Aug. 1997.
[30] J.-C. Pearson, P. Chen, and H.-M. Pickett, "Photomixer systems as submillimeter oscillators and coherent test sources," in *Proc. SPIE—Millimeter Submillimeter Detect. Astron.*, Feb. 2003, vol. 4855, pp. 459–467.
[31] S. Ristic, A. Bhardwaj, M. J. Rodwell, L. A. Coldren, and L. A. Johansson, "An optical phase-locked loop photonic integrated circuit," *IEEE/OSA J. Lightwave Technol.*, vol. 28, no. 4, pp. 526–538, Feb. 2010.
[32] Y.-S. Wu, J.-W. Shi, and P.-H. Chiu, "Analytical modeling of a high-performance near-ballistic uni-traveling-carrier photodiode at a 1.55μm wavelength," *IEEE Photon. Technol. Lett.*, vol. 18, no. 8, pp. 938–940, Apr. 2006.
[33] J.-W. Shi, C.-Y. Wu, Y.-S. Wu, P.-H. Chiu, and C.-C. Hong, "High-speed, high-responsivity, and high-power performance of near-ballistic uni-traveling-carrier photodiode at 1.55 μm wavelength," *IEEE Photon. Technol. Lett.*, vol. 17, no. 9, pp. 1929–1931, Sep. 2005.
[34] W.-L. Lee, K.-C. Wu, J.-Y. Jiang, and J. Lee, "A laser ranging radar transceiver with modulated evaluation clock in 65 nm CMOS technology," in *Proc. Symp. VLSI Circuits Dig. Tech. Papers*, Kyoto, Japan, Jun. 2011, pp. 286–287.